Time-Controlled SPAD Receivers in Optical Wireless Communication System

Junzhi Liu, *Student Member, IEEE*, Wei Jiang, *Member, IEEE*, Shiva Kumar, *Member, IEEE*, and M. Jamal Deen, *Life Fellow, IEEE*

***Abstract*—Single-photon avalanche diodes (SPADs) capable of single photon detection are promising optical sensors for use as receivers in optical wireless communication (OWC) systems. In SPAD-based receivers, the intersymbol interference (ISI) effect caused by dead time is an important drawback that limits performance. In this paper, we propose two novel SPAD operation modes to reduce the ISI effect in SPAD-based OWC. To validate the feasibility of these two modes, we designed a free-running SPAD front-end circuit with post-layout transient simulation results and some measurements to show its function and performance. This SPAD circuit is improved by a novel mixed passive-active quench and reset front-end circuit that achieves a very short dead time. Based on the traditional free-running mode, we design the clock-driven mode and time-gated mode to reduce the ISI effect through time-controlled operating signals. To accurately evaluate these three modes, we develop a new simulation system to assess the ISI effect in On-Off Keying (OOK) modulated communication. The simulation results demonstrate that the clock-driven mode and time-gated mode receivers can improve the bit error rate (BER) performance in low data rate communication and high data rate high optical power communication, respectively. Moreover, compared to the free-running mode, the two proposed time-controlled modes achieve higher data rate communication and better noise tolerance ability in SPAD-based OWC.**

***Index Terms*—Single-photon avalanche diode (SPAD), optical wireless communication (OWC), intersymbol interference (ISI), on-off keying (OOK), bit error rate (BER).**

I. Introduction

With the development of optical wireless communication (OWC), high-speed transmission, high stability and low power consumption have become important research topics. Single-photon avalanche diode (SPAD) has attracted considerable interests as the receiver in OWC systems due to its high sensitivity and accurate timing resolution [1]. For example, a SPAD-based receiver achieved 117 m transmission distance and 2 Mbps data rate communication in an underwater OWC application [2]. A 64 × 64 SPAD receiver manufactured in complementary metal-oxide semiconductor (CMOS) technology was used in an OWC system for 500 Mb/s data rate transmission with only −46.1 dBm received optical power [3]. The maximum 3.45 Gbit/s data rate with on-off keying (OOK) and 5 Gbps with orthogonal frequency division multiplexing (OFDM) were demonstrated using commercial SPAD arrays [4], [5].

A SPAD is a p-n junction with a reverse bias above its breakdown voltage, thus generating a large electric field across the depletion region [6]. In such a high electric field, self-sustained avalanche can be triggered by even a single carrier (photon or dark noise) [7]. For each avalanching event, the SPAD needs time for quenching and resetting to complete the full detecting cycle, which is called the dead time [8]. During the dead time, the SPAD cannot respond to other incident photons. SPADs with active quench and reset (AQR) circuit have a hold-off time between the quench and reset process to reduce the secondary dark counts, which is also called afterpulsing effect [9]. By varying the hold-off time, one can adjust the duration of the dead time. [7]. In a SPAD-based optical receiver, dead time determines its operating frequency, thus having a great impact on its bit error rate (BER) performance [10].

SPAD pixels can be reset or disabled periodically by a clock, which is called a clock-driven (CD) SPAD. In a SPAD with the AQR circuit, the active quench and active reset can be controlled to implement the quench and reset processes, respectively. With the support of CD mode, SPAD pixels can respond to periodic photon events and keep inactive for noise photons. In the recent publications, the CD mode SPAD was used in image sensor and image scanning microscopy applications, showing higher counting efficiency and higher linearity [11], [12]. Currently, there are very few applications in CD mode SPAD-based OWC receiver. The time-gated (TG) mode of SPAD operation can be achieved through selectively adjusting the biasing voltage to exceed or fall below the SPAD breakdown voltage within designated time intervals [13], [14]. Our proposal to use the TG mode to improve the performance of SPAD-based OWC systems was presented in [15]. The gating signals turn the SPADs on and off regularly in each bit interval, which means that the SPADs can only detect photons in the gate-ON time and are inactive in gate-OFF time slot. Inter-symbol interference (ISI) can be mitigated by the gating signals because SPAD has no response to incident photons during gate-OFF, thus reducing the photon counting rate and alleviating the ISI effect caused by the dead

Manuscript received 17 August 2023; accepted 24 August 2023. Date of publication 8 September 2023; date of current version 21 September 2023. This work was supported in part by the Natural Science and Engineering Research Council of Canada and in part by CMC Microsystems. *(Corresponding author: M. Jamal Deen.)*

Junzhi Liu, Wei Jiang, and Shiva Kumar are with the Department of Electrical and Computer Engineering, McMaster University, Hamilton, ON L8S 4K1, Canada (e-mail: liu1329@mcmaster.ca; jiangw35@mcmaster.ca; skumar@mcmaster.ca).

M. Jamal Deen is with the Department of Electrical and Computer Engineering, McMaster University, Hamilton, ON L8S 4K1, Canada, and also with the School of Biomedical Engineering, McMaster University, Hamilton, ON L8S 4K1, Canada (e-mail: jamal@mcmaster.ca).

Digital Object Identifier 10.1109/JPHOT.2023.3309881

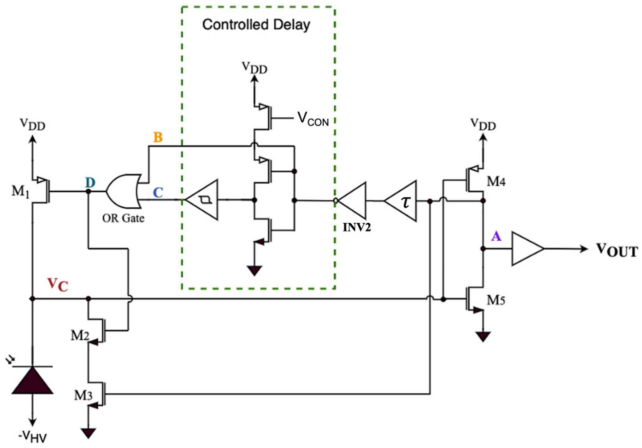

Fig. 1. Schematic of the front-end SPAD circuit.

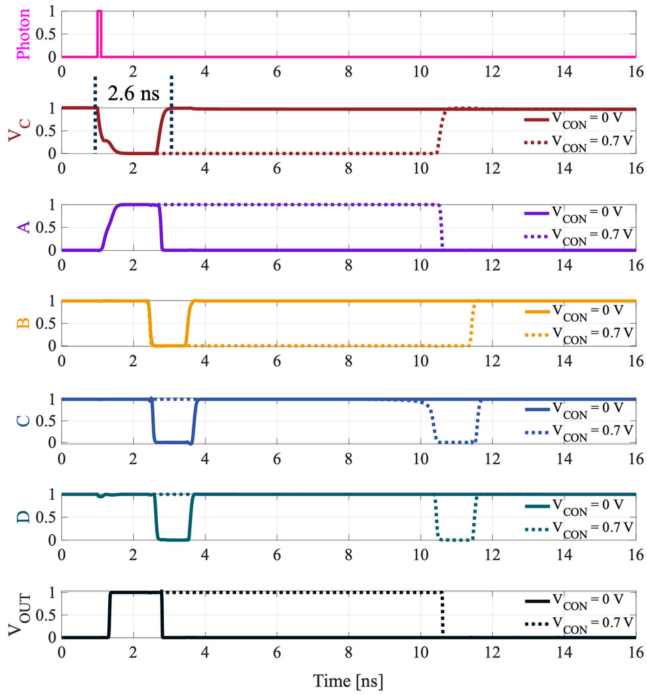

Fig. 2. Post-layout transient simulation results for the SPAD circuit.

time [15]. Another research challenge in a TG SPAD receiver is to reduce ISI effects by adjusting the gate-ON slot to an optimal value in AQR SPADs [16].

In this paper, we designed two types of SPAD-based receivers, and developed a communication model to verify the functions of the two receivers. To the best of our knowledge, the CD SPAD is used in the OWC field for the first time in this work. A new model based on Monte Carlo simulation is first designed to evaluate the block time and present the relationship between optical power and the ISI effect. The simulation results show that, compared with the traditional free-running (FR) SPAD receiver, our proposed CD and TG receiver can effectively improve the performance of the SPAD-based OWC system. The basic front-end circuit with very low dead time and two derived novel CD and TG operation modes are introduced in Section II. The photon counting analysis of FR SPAD receiver, CD-mode SPAD and TG-mode SPAD receivers are presented in Section III. The BER evaluation is simulated and demonstrated in Section IV. Finally, the conclusions are provided in Section V.

II. SPAD Front-End Circuits

In this section, a SPAD front-end circuit is designed in a 65 nm standard CMOS technology and some measured results are presented. The CD mode and TG mode SPAD circuits are derived from the basic FR circuits. These circuits with time-controlled functions are then used to design CD mode and TG mode receivers for low data rate OWC and high data rate OWC applications, respectively, utilizing two different signal generation circuits. Post-layout transition simulations demonstrate that implementing the two modes (CD mode and TG mode) can significantly reduce the block time in the SPAD receiver compared to the FR mode.

A. Basic Front-End Circuit for SPAD

The schematic of the basic front-end circuit is shown in Fig. 1, and two post-layout simulation results under two control voltages (V_{CON}) are shown in Fig. 2. The SPAD model in the simulation comes from our previous work [8]. Initially, the cathode voltage of the SPAD V_C is at 1 V and the anode is connected to $-V_{HV}$ to bias the SPAD above the breakdown voltage. M4 and M5 form an inverter to keep node A at low voltage, causing M3 to be off. The 0.8 ns fixed delay element τ, the second inverter and the controlled delay element are connected in series to keep node B and node C in high voltage. Node D is at 1 V due to the OR gate. Therefore, M2 turns on and M1 is off. In this initial condition, the SPAD is biased above the breakdown voltage, and it is in the photon detecting mode.

When an incident photon is detected, self-sustaining avalanche initiates, M3 in the off-state acts as a large resistance to generate a passive quench process and reduces the voltage of V_C. The inverter made by M4 and M5 senses the declining V_C and reverses the node A to a high voltage level, hence turning M3 on to start an active quench process. The bias voltage will become below the breakdown voltage when V_C connects to ground through M2 and M3, starting the hold-off process. The rising voltage of node A will be delayed by τ and reversed by the second inverter INV2, causing a change on node B. The falling edge of the voltage in node B is delayed by the controlled delay element and the node C is the output of the delay element. At the moment when both nodes B and C turn to low voltage level, the OR gate will change node D to low voltage level and turn M2 off and M1 on, so the hold-off process will be terminated and the SPAD will be recharged back to its initial state through M1. The inverter made by M4 and M5 senses the high voltage of V_C and then changes the node A to a low voltage, which results in node B turns to high voltage after the time τ and terminates the reset process. Then, the SPAD pixel is ready to detect the next photon. The time τ here is designed to be 0.8 ns, thus having enough time for the reset process and the hold-off process. One buffer is connected to node A to generate the output pulse V_{OUT}. The controlled delay element consists of a voltage-controlled

inverter and a Schmitt trigger, which only delays the falling edge of node B. This feature ensures that the hold-off time can only be delayed by the controlled delay element and has no effect on other processes. The delay duration of the controlled delay element increases with the increasement of V_{CON}.

As shown in Fig. 2, the dead time can be observed by the V_C variance, and the shortest achievable dead time of the basic front-end circuit is 2.6 ns when the V_{CON} is 0 V. For comparison, the dead time is 10 ns when V_{CON} is set to be 0.7 V. The quench and the reset times are 0.7 ns and 0.8 ns, respectively, in both V_{CON} conditions. Hold-off time is 1.1 ns when V_{CON} is 0 V, and increases to 8.5 ns when V_{CON} is set to be 0.7 V.

For the OWC application, a short dead time leads to a high photon detection ability, thus increasing performance of a SPAD-based OWC receiver [10]. In contrast, a long dead time will cause the ISI effect and disturb the photon counting process in an OWC system [17]. In this design, the shortest achievable dead time is 2.6 ns, which is much shorter than some of recently reported values (8–30 ns) [18], [19], [20]. To achieve a short dead time, we need to reduce the hold-off time. However, a lower hold-off time may cause a higher afterpulsing probability [21], [22], which decreases performance of OWC systems. The controlled delay element in our design can be used to adjust the hold-off time to an optimal value to balance the noise effect and photon detection ability.

B. Clock-Driven Mode of SPAD Circuit

In the CD mode SPAD receiver, a new reset mechanism is designed to reset the SPAD by both the CD signal and the AQR circuit. Fig. 3 shows the schematic of the CD signal generation circuit, CD mode front-end circuit and the layout. The post-layout transient simulation results of these circuits are shown in Fig. 4. In Fig. 3(a), the CD signal generation circuit consists of one NAND gate, one inverter and one fixed delay element which has a same delay time with the fixed delay element τ in the basic front-end circuit as shown in Fig. 1. The circuit input (data signal) is designed to have a same frequency of the data rate and can be implemented through the bit synchronization technology [23]. The CD signal can be described as a periodic pulse generated at the beginning (the rising edge of the data signal) of every bit interval as shown in Fig. 4. The length of the CD signal pulse is determined by the fixed delay element τ to ensure enough reset time for the SPAD pixel.

In Fig. 3(b), an added transistor M_{S1} connects with M1 in parallel and M_{S2} connects with M2 and M3 in series. As a result, the low voltage level of the CD signal turns M_{S2} off and M_{S1} on, which disconnects the cathode to the ground while connecting the cathode to VDD. That is, the CD signal can disable the hold-off process and recharge the SPAD back to initiate, the reset process at the beginning of every bit interval.

The post-layout transient simulation results of the CD-mode SPAD pixel are shown in Fig. 4. The solid line in the fourth sub graph (iv) is the waveform of V_C under the CD mode, and the dotted line is the waveform of the V_C in the FR mode. V_{CON} is set to 0.7 V to adjust the dead time of the SPAD pixel to be 10 ns to balance the performance of dark count rate (DCR) and

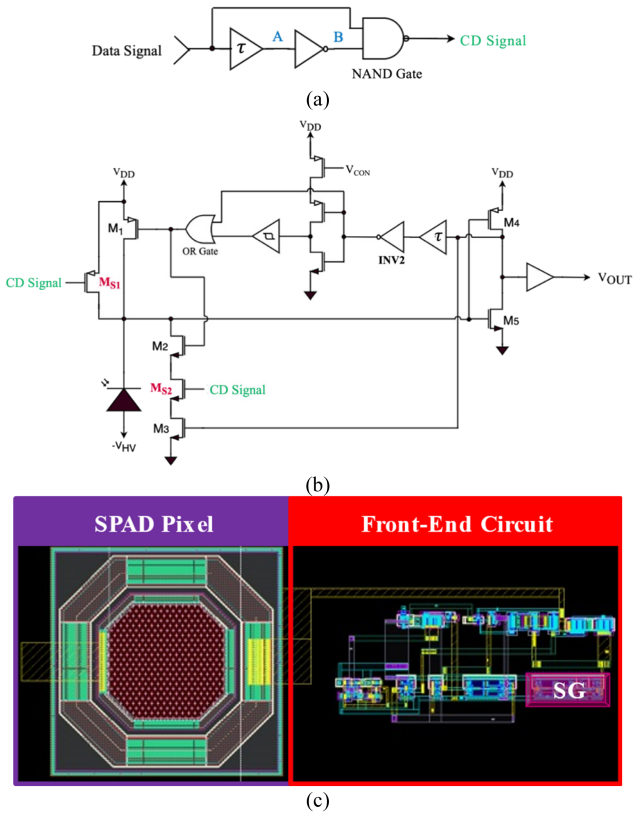

Fig. 3. (a) Schematic of the clock-driven (CD) signal generation circuit. (b) Schematic of the front-end circuit in the clock-driven (CD) mode. (c) Layout of the clock-driven (CD) mode circuit in a standard 65 nm CMOS process.

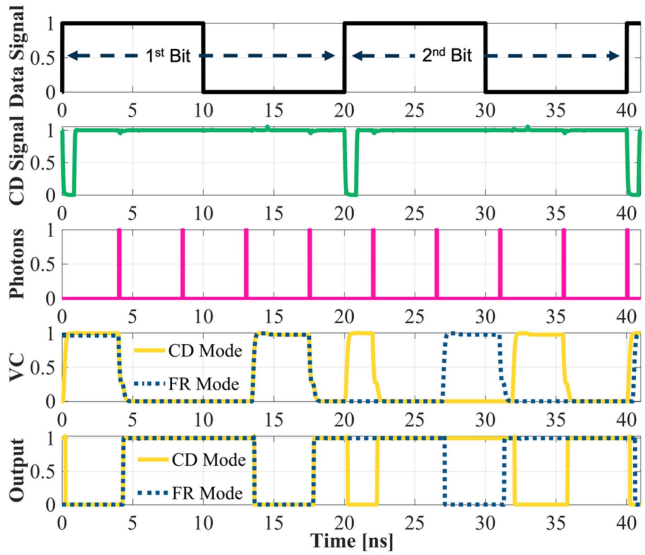

Fig. 4. Post-layout transient simulation results for the signal generation circuit, the clock-driven (CD) mode front-end SPAD circuit and the free-running (FR) mode front-end circuit.

photon counting ability. The bit interval is set to 20 ns. In CD mode, the dead time that caused by the detected photon or dark carrier in one bit interval will not affect the photon counting ability of the SPAD in the next consecutive bit interval due to the reset process at the beginning of every bit interval. In

this mode, the photon counting process in every bit interval is independent, and the dead time is not fixed, but determined by the moment when photons arrive. In the Fig. 4, FR mode has a fixed dead time. However, in the CD mode, the dead time caused by the first detected photon is 10 ns and the next dead time in CD mode is only 2.1 ns. As a result, the SPAD pixels have a lower average dead time in the CD mode. It is worth emphasizing that the dead time in CD mode cannot be infinitely short. Although the hold-off time can be set to 0, the quench and reset times (approximately 1.5 ns) need to be preserved to ensure the continuous detection capability of the SPAD. Compared to the FR mode, a SPAD receiver in the CD mode has a higher photon counting ability. For example, a SPAD under the CD mode counted 4 photons during two bits, but FR mode counted only 3 photons under the same photon incident condition as shown in Fig. 4. Another advantage of using the CD mode is the reduction of ISI effect since the dead time does not extend to the next bit. As shown in the Fig. 4, the dead time caused by the incident photon in the 1st bit extends to the 2nd bit, thus leading to an ISI effect. In contrast, the CD mode resets the SPAD pixels at the beginning of bit interval, thus significantly reducing the ISI effect. This feature improves the performance of SPAD receiver significantly in OWC system. It is worth noting that, in a high data rate condition, the afterpulsing rate may increase because of the CD-mode operation resets the SPAD pixels at a high frequency, leading the average hold-off time to be low in the high data rate condition. This is due to that a short hold-off time can strongly increase the afterpulsing rate.

C. Time-Gated Mode of SPAD Circuit

The time-gated mode SPAD is designed for the high data rate communications, where the bit interval is shorter than the dead time. Fig. 5 shows the schematics of the TG signal generation circuit, the TG mode front-end circuit and the layout. As shown in Fig. 5(a), the TG signal generation circuit is made of three D flip-flops, four 3-inputs OR gates, several inverters and buffers. The TG signal generation circuit generates four TG signals and divides a full SPAD array into four sub-SPAD arrays. In our design, the full SPAD array is set to be 64 SPAD pixels and every sub-SPAD array has 16 SPAD pixels. The schematic of the TG mode front-end circuit is shown in Fig. 5(b). In contrast to the CD mode, M_{S1} connects with M1 in series and M_{S2} connects with M2 and M3 in parallel. The SPAD pixels stay in hold-off during the high voltage of TG signal since M_{S1} turns off and M_{S2} turns on. Under this condition, the cathode of SPAD connects to ground through M_{S2}. The low voltage of TG signal enables the SPAD pixels to the active detection condition because the M_{S2} is turned off and the M_{S1} is turned on, thus recharging the cathode of the SPAD. As a result, the TG signal enables every sub-SPAD array to be turned on by the gate-on signal and turned off by the gate-off signal.

In this TG mode, 4 TG signals continuously operate four sub-SPAD arrays and one TG signal only operates one specific sub-SPAD array. Fig. 6 shows the 4 TG signals generated in sequence and form a cycle and the length of gate-on intervals

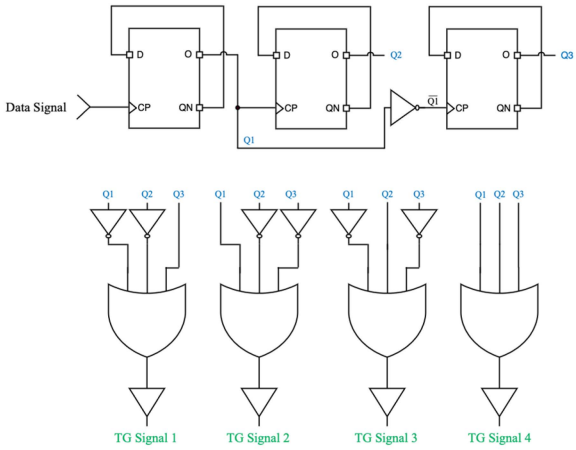

(a)

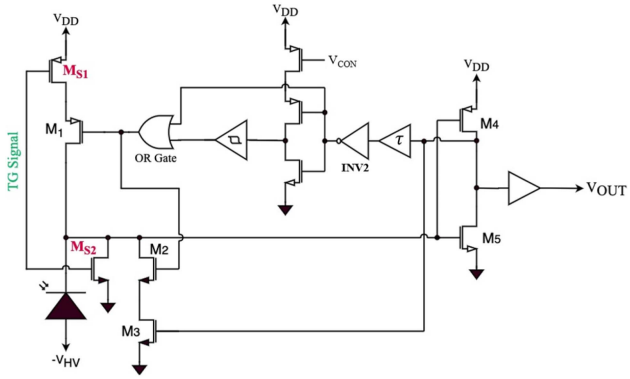

(b)

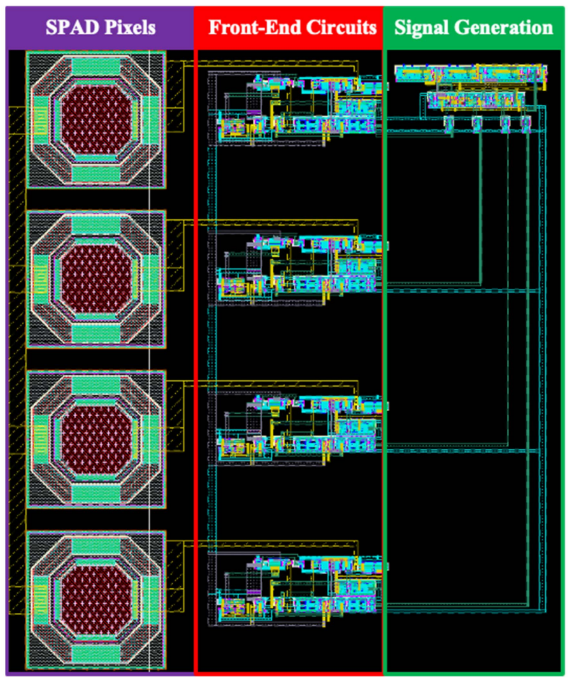

(c)

Fig. 5. (a) Schematic of the time-gated signal generation circuit. (b) Schematic of the front-end circuit in the time-gated mode. (c) The layout design of the time-gated (TG) mode circuit.

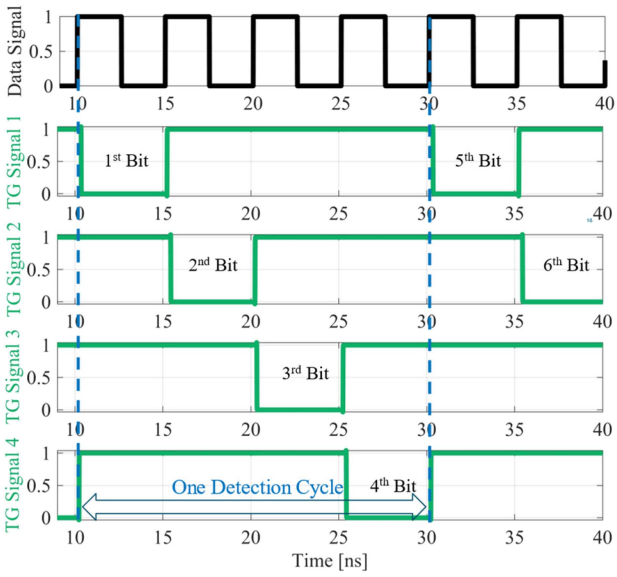

Fig. 6. Post-layout transient simulation results for the time-gated (TG) signal generation circuit.

from TG signals (low voltage level) is as same as the bit interval. One detection cycle contains four sub-SPAD arrays being enabled cyclically by four TG signals. Therefore, one sub-SPAD array only detect one bit in one detection cycle and 4 bits can be detected in one detection cycle in total. In the TG mode, every sub-SPAD array is independent and there is always a sub-SPAD array at the gate-on interval due to the cyclic enablement function. When the dead time is less than 4 times of the bit interval, there is no ISI effect in the TG mode because the dead time in one sub-SPAD array cannot cause any effect on other sub-SPAD arrays. However, if the dead time is above 4 times of the bit duration, the dead time in one sub-SPAD array may extend to the next detection cycle, leading to the ISI effect in this sub-SPAD array.

In the simulation of the TG mode front-end circuit, the dead time is set to be 10 ns and bit interval is set to be 5 ns for high data rate communication. Under these conditions, every SPAD pixel can detect at most one photon in one bit interval. The post-layout transient simulation is shown in Fig. 7, where the four SPAD pixels operate as four sub-SPAD arrays enabled cyclically by four TG circuits. Compared to the FR mode, the TG mode receiver detects 4 photons over the 4-bit intervals, and the FR mode receiver can detect up to 8 photons but cannot detect any photon in the second and third bits due to the ISI effect. In contrast, the TG mode receiver detects one photon in every bit interval with no ISI effect. Also, compared to the FR mode, the equivalent detection time of TG mode is extended since the dead time in one channel does not affect the other channels. While the photon counting rate may reduce in TG mode, it significantly improves the detection interval consistency in optical wireless communication and has a potential to perform better than the traditional FR mode when ISI effect is very serious.

In some past research on SPAD-based OWC, the time-gated mode was primarily applied to PQR SPADs to control the extension of the dead time. In the application described in [11],

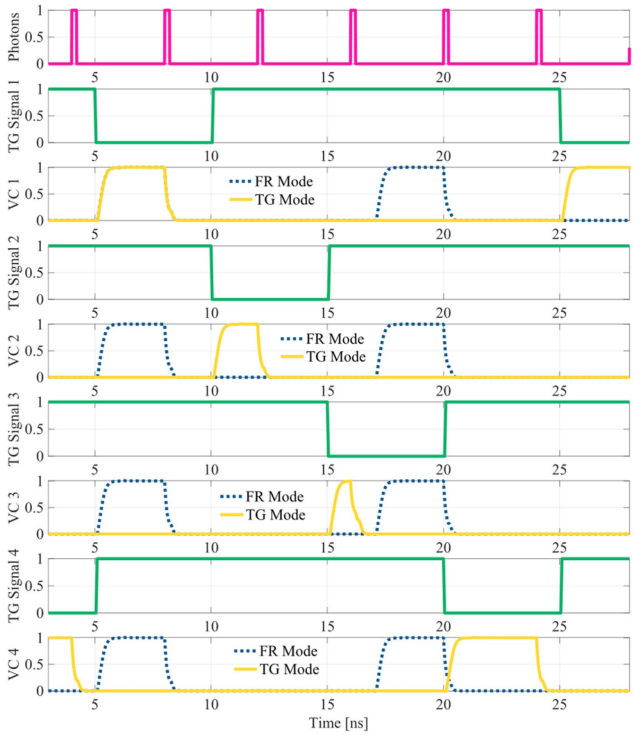

Fig. 7. Post-layout transient simulation results for the time-gated (TG) mode SPAD front-end circuit and free-running (FR) mode SPAD front-end circuit.

the SPAD is forced off through gate-off signals, resulting in a significant reduction in the photon counting capability due to the prolonged dead time under high-intensity light conditions. Our research focuses on AQR SPADs with the aim of reducing the ISI effect in high-speed communication environments by utilizing the gate-off operation to enable partitioned detection across the entire SPAD array. This approach helps to minimize the block time and effectively mitigate the impact of ISI on the SPAD's performance.

D. Circuit Test

To measure functions of the circuits, the proposed SPAD front-end circuits are fabricated in the standard TSMC 65 nm process. The measurement setup is shown in Fig. 8. A printed circuit board (PCB) was designed to offer the interfaces for the power supplies, input clock signals and SPAD outputs. An Agilent E3646A DC power supply was used to provides the necessary voltage supplies for the measurement. A LED with a wavelength of 430 nm is operated by a Hewlett Packard 3325B function generator to provide the light source. When the clock is at high level of 3.3 V, the LED is on and illuminates the SPAD pixel. When a low level of 0 V is applied, the LED will be off. To validate the basic function of the SPAD pixel, we biased the SPAD at 10.35 V, adjusted VCON to be 0.7 V, configured the SPAD in the FR mode, and set the LED-driven clock to be 200 kHz. In this measurement condition, when the clock is at a high level, the SPAD pixel is illuminated, resulting in a significant number of output pulses. However, when the clock is at a lower level, the LED is off and only a few numbers of pulses can be

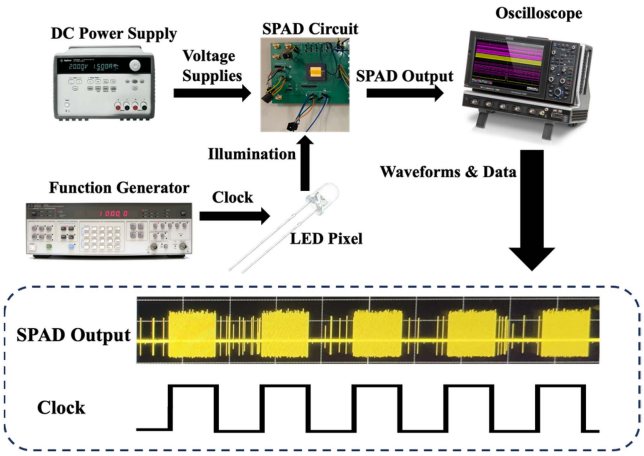

Fig. 8. Diagram of the experimental setup for SPAD circuit measurement.

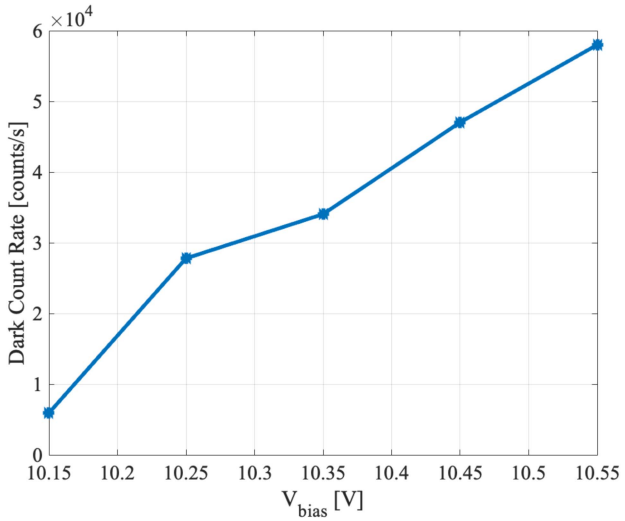

Fig. 9. Dark count rate of proposed SPAD receiver under different bias voltage.

observed. Those pulses are mainly due to the background noise and dark noise. As shown in Fig. 8, the waveform of the SPAD pixel output indicates that the circuit functioned correctly.

In addition, we measured two other key performances of the SPAD pixel: DCR and photon count rate. In the DCR measurement, we shielded the SPAD receiver with a metal sheet cover and conducted measurements in a dark room to ensure a dark environment. The SPAD was configured in the basic FR mode, with the control voltage V_{CON} set to be 0 V to achieve the lowest dead time. The DCR values were obtained by averaging the time interval between two dark counts. Each DCR value was calculated from at least 10^5 dark count measurements to ensure its accuracy. The Fig. 9 illustrates the DCR results when varying the bias voltage. As shown in Fig. 9, the DCR gradually increased from 5.9×10^3 Counts/s to 5.8×10^4 Counts/s when the bias voltages changed from 10.15 V to 10.55 V.

The dead time of SPAD significantly affects its photon count rate. As described in the Section II-A, the dead time of proposed SPAD is controlled by the V_{CON} and increases with the higher control voltage settings. In the photon count rate measurement, the clock in Fig. 8 was replaced by a constant voltage (3.3 V).

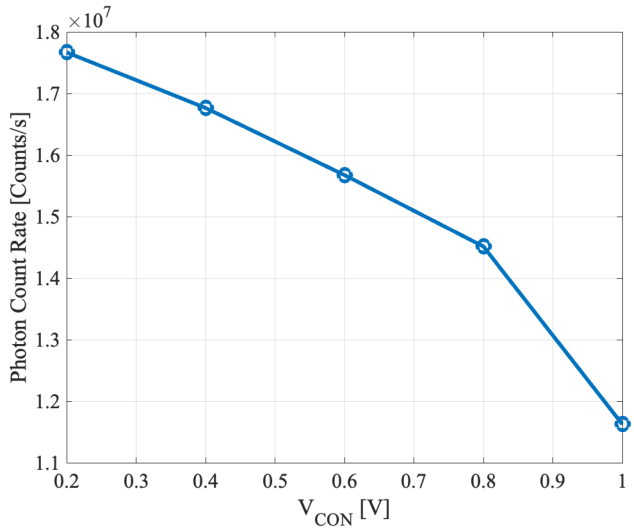

Fig. 10. The photon count rate of designed SPAD receiver under different control voltage (V_{CON}).

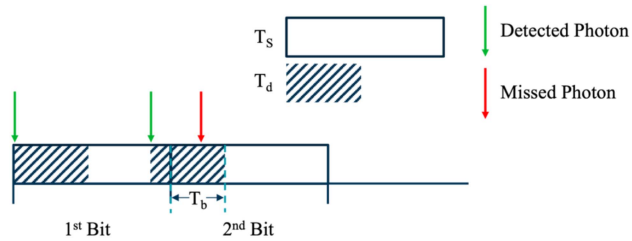

Fig. 11. Diagram of block time generation process.

That is, the LED provided a continuous and constant light source for the SPAD pixel. The V_{CON} is varied from 0.2 V to 1 V with a step size of 0.2 V. The related photon count rates at each V_{CON} were measured. As shown in Fig. 10, the photon counting rates of the SPAD decreases with the increase of the control voltage with the same optical power level of the LED light source. This is because the higher control voltage leads to an increased dead time, reducing the effective detection time of the SPAD and the probability of photon detection [5].

III. Photon Counting Analysis of SPAD Receivers

A. Analysis and Simulations of the Block Time

As mentioned in Sections II-B and C, the dead time of SPAD may cause ISI effect in the FR mode, thus degrading the receiver performance. Fig. 11 demonstrates the block time generation process. T_S is the bit interval; T_d is the dead time and T_b is the block time. The last detected photon in the first bit causes the dead time, but this dead time may extend to the second bit and cause an inactive interval. This is the process of how the block time is generated [24]. Due to the existence of the block time, the effective photon detection time of every bit will be reduced to T_S-T_b, thus resulting in a reduced photon counting in an OWC system.

For a SPAD receiver, the arrival time of the incident photon is random and follows the Poisson arrival process [25]. As a result, the block time of every SPAD pixel in each bit of the OWC

system is different even under the same condition. To solve this problem, Monte Carlo simulation is introduced to obtain the numerical analysis of the block time. The block time in one bit interval is mainly determined by the detected time of the last detected photon in the previous bit interval. For example, in Fig. 11, the last detected photon in the 1st bit leads to the block time T_b in the 2nd bit. Therefore, the focus of Monte Carlo simulation is to analyze the detected time of the last detected photon in the first bit interval.

For the first step of the block time simulation, the photon counting probability in the first bit (no ISI effect) is needed to analyze the number of detected photons in the 1st bit, which can be expressed as [25], [26]:

$$p_K(k) = \begin{cases} \sum_{i=0}^{k} \psi\left(i, \lambda_k\right) - \sum_{i=0}^{k-1} \psi\left(i, \lambda_{k-1}\right) & k < k_{\max} \\ 1 - \sum_{i=0}^{k-1} \psi\left(i, \lambda_{k-1}\right) & k = k_{\max} \\ 0 & k > k_{\max} \end{cases} \tag{1a}$$

$$k_{\max} = \frac{T_s}{T_d} + 1 \tag{1b}$$

$$L = \frac{PDE \times P_O}{N h f_0} \tag{1c}$$

where the function $\psi(i,\ \lambda)$ is defined as $\psi(i,\ \lambda)\ = \lambda^i\ e^{-\lambda}/i!$, and $\lambda_k = L(T_S - kT_d)$; k is the number of detected photons, $k_{\max}$ is the maximum value of k and L is the average photon detection rate (photons/s). P_O is the received optical power, N is the number of SPAD pixels in a SPAD array, *PDE* is the photon detection efficiency, h is the Planck constant and f_o is the frequency of the incident photons. For the consistency of the simulation results, we refer to our previous research [15] and set N to be 64, T_d to be 10 ns, *PDE* to be 38%, and f_0 to be 7.138×10^{14} Hz (wavelength = 420 nm) in all the following simulations (Figs. 12 to 20). The mean and variance of the photon counting probability distribution for the first bit are [25]:

$$\mu_k = k_{\max} - \sum_{k\ =\ 0}^{k_{\max}-1} \sum_{i\ =\ 0}^{k} \psi\left(i, \lambda_{k-1}\right) \tag{2a}$$

$$\sigma_k^2 = \sum_{k=0}^{k_{\max}-1} \sum_{i=0}^{k} \left(2k_{\max} - 2k - 1\right) \psi\left(i, \lambda_{k-1}\right) - \sum_{k\ =\ 0}^{k_{\max}-1} \sum_{i\ =\ 0}^{k} \psi\left(i, \lambda_{k-1}\right) \tag{2b}$$

As the value of photons detected, k in the first bit can be used to analyze the possible time of the last detected photon in the first bit and the photon counting distribution can be used as the probability distribution to calculate the block time (T_b) of The FR mode SPAD receiver suffers from the short the second bit, which can be expressed as:

$$T_b = \max\left\{T_d - rand\left(0,1\right) \times \left[T_s - \left(k-1\right) T_d\right],\ 0\right\} \tag{3}$$

Although the probability of the total number of detected photons k can be calculated, the detection time of each photon is still random. The term $rand(0,1) \times [T_s - (k-1)]T_d$ represents the detected time of the last detected photon in the first bit interval.

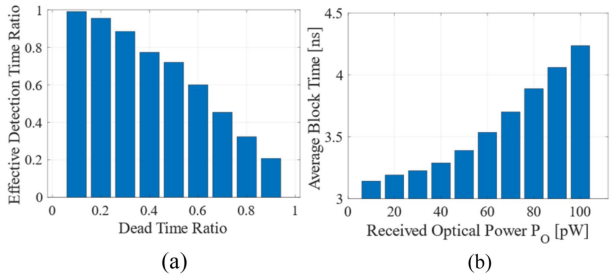

Fig. 12. (a). The average block time ratio of the variant dead time ratio when $P_O = 60$ pW, and (b), the average block time of the variant received optical power when $T_b = 10$ ns and $T_S = 20$ ns.

The average block time can be calculated after 10^6 times simulations to ensure the accuracy. The results are shown in Fig. 12. The dead time ratio is defined as T_d/T_s, which is a parameter to show the dead time effect in a OWC system. The effective detection time ratio is defined as $(T_s - T_b)/T_s$, serves as a parameter to quantify the impact of ISI, with a lower effective detection time ratio indicating a more pronounced ISI effect. In Fig. 12(a), a negative correlation is observed between the dead time ratio and the effective detection time ratio, suggesting that the dead time significantly influences the block time. For example, when the dead time ratio is large it can lead to a serious ISI effect in the OWC system. The block time increases with the increase of the received optical power as shown in Fig. 12(b). This is because that a higher chance for photons to arrival at the end of first interval will result in a higher probability of extending the dead time to the second bit interval.

The FR mode SPAD receiver suffers from the short effective detection interval because the block time occupies a faction of total bit interval. For a SPAD array, every SPAD pixel is an independent photon counter. As a result, the block time is different for different SPAD pixels. Based on the (2) and (3), the mean and variance of photon counting probability distribution in a free-running SPAD array can be written as:

$$\mu_{kf} = \sum_{j=1}^{N} \left[k_{\text{maxj}} - \sum_{k=0}^{k_{\text{maxj}}-1} \sum_{i=0}^{k} \psi\left(i, \lambda_{(k-1)j}\right)\right] \tag{4a}$$

$$\sigma_{kf}^2 = \sum_{j=1}^{N} \left[\sum_{k=0}^{k_{\text{maxj}}-1} \sum_{i=0}^{k} \left(2k_{\text{maxj}} - 2k - 1\right) \psi\left(i, \lambda_{(k-1)j}\right) - \sum_{k=0}^{k_{\text{maxj}}-1} \sum_{i=0}^{k} \psi\left(i, \lambda_{(k-1)j}\right)\right] \tag{4b}$$

$$k_{\text{maxj}} = \left(T_s - T_{bj}\right)/T_d\ + 1 \tag{4c}$$

$$\lambda_{kj} = L\left(T_s - T_{bj} - kT_d\right) \tag{4d}$$

where k_{maxj} is the maximum number of the counted photons for the jth SPAD pixel and T_{bj} is the block time of the jth SPAD pixel, the μ_{kf} and σ_{kf}^2 are the summation of all the counting means and counting variances from the single SPAD pixel in a SPAD array.

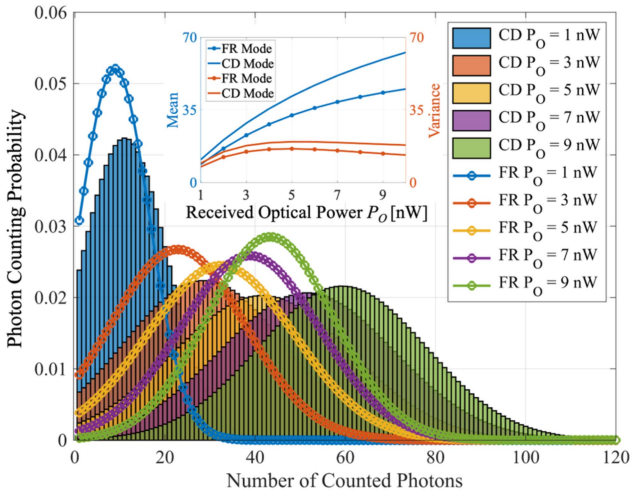

Fig. 13. Photon counting probability distribution variances of the clock-driven (CD) mode and the free-running (FR) mode with the increased optical power (64-SPAD array with 10 ns dead time and 15 ns bit interval).

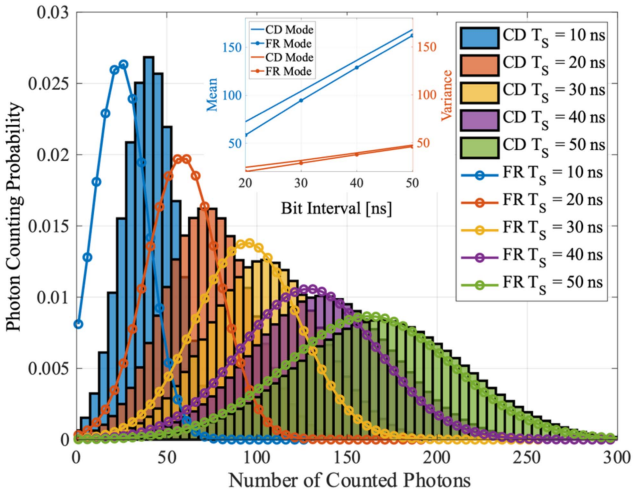

Fig. 14. Photon counting probability distribution variances of the clock-driven (CD) mode and the free-running (FR) mode with the increased bit interval (T_S) when $P_O = 8$ nW (64-SPAD array with 10 ns dead time).

B. Clock-Driven Mode Receiver

As introduced in Section II-B, the CD mode SPAD receiver can reset SPAD from the hold-off status. Therefore, no dead time can extend to the next bit interval. That is, the effective detection times of every bit interval are equal. The photon counting probability distribution of every bit interval in CD mode follows (1a), which has no ISI effect. Compared to the FR-mode SPAD receiver, the SPAD operated in CD mode has the advantage of no ISI effect brings longer effective detection time. Therefore, the CD-mode SPAD has a higher photon detection ability than the FR mode.

The photon counting probability distributions based on unmodulated signals can be observed in Figs. 13 and 14. In Fig. 13, with the increase of the received optical power (P_O), the number of detected photons increases, leading to the photon counting probability distributions of the CD and FR modes moving to the right, which represents higher mean values. In the high optical power condition ($P_O = 9$ nW), a significant gap exists between the CD mode and the FR mode due to the higher average values of counted photons in the CD mode. The mean value of the photon counting distribution represents the average photon counting rate for a SPAD receiver. Comparing the mean values shows an increasing gap with the increase of P_O, as shown in the inserted figure in Fig. 13. It can be explained that the degree of the ISI effect becomes more and more serious with the increase of optical power. But it is worth noting that the mean value still increases with the increase of P_O in the CD mode, because the improvement of system performance by the higher photon count rate exceeds the deterioration of system performance by ISI effect. For the variance values, the CD mode has a higher value than the FR mode. This is because the CD mode has a longer effective photon detection time, while the FR mode has a shorter effective photon detection time than the CD mode due to the ISI effect. With the increase of P_O, the photon detection time in the FR mode will be shorter and shorter, causing the gap between the variance values of CD and FR to also increase with the increase of P_O. In Fig. 13, when P_O is 1 nW, the variance value of the CD mode distribution is 9.42, while that of the FR mode is 7.66. However, when P_O is 9 nW, the variance value of the CD distribution is 18.48, while that of the FR mode is 14. In the case of $T_S > T_d$, the gap in variance values of the two modes does not change too much with the increase of P_O. This is because the block time is not long compared to the entire bit interval.

Fig. 14 shows the photon counting probability distributions variance with different bit intervals (T_S). The increased T_S values lead to a smaller dead time ratio. In addition, the difference between the CD mode distribution and the FR mode distribution in large bit interval ($T_S = 50$ ns) is small. This is because the block time is short enough, thus the ISI effect can be ignored in the FR mode. The inserted figure in Fig. 14 shows an approaching trend of two mean values with the increase of the bit interval, which indicates that the ISI effect on the FR receiver gets smaller with the increase of the bit interval. In the case of a short T_S($T_S = 20$ ns), a gap in variance between CD and FR distributions can be observed (24.49 for the CD mode and 20.11 for the FR mode). The reason for this gap is because the receiver has a longer effective detection time in the CD mode, resulting in a larger variance value. On the contrary, when $T_S = 50$ ns, the distributions of the two modes are highly coincident, which means that the gap in the variance value almost disappears. This is because the very long T_S causes the proportion of block time in the entire bit interval becoming very small, thus making the ISI effect negligible.

The probability distributions in Figs. 13 and 14 demonstrate that the CD-mode SPAD receiver has a higher photon counting ability than the FR mode, especially under high optical power or low bit interval conditions. This is because that the CD mode is not affected by the block time under these two conditions. These features make the CD mode to have better performance than the traditional FR mode in OWC system.

C. Time-Gated Mode Receiver

The TG signal operates four sub-SPAD arrays for the high data rate condition, in which the dead time is longer than the bit interval. In this condition, the block time for one single SPAD pixel can cover several entire bit intervals and the FR mode is no longer accurately described by (4). Instead, the photon counting process can be modeled as a Bernoulli process with two states for each SPAD pixel [10]. State 1 for blocking, which indicates that no incident photon can be detected and state 0 for detection, where at most one incident photon can be possibly detected [27]. The Markov chain can be used to model the photon counting process. The mean μ'_k and variance σ'^2_k of the photon counting probability distribution for the FR mode in high data rate condition can be expressed as [10], [27]:

$$\mu'_k = N\frac{LT_S}{1+mLT_S} \tag{5a}$$

$$\sigma'^2_k = N\frac{LT_S+(m-1)L^2T_S^2}{(1+mLT_s)^2} \tag{5b}$$

$$m = \frac{T_d}{T_S} \tag{5c}$$

where N is the number of SPAD pixels in a SPAD array, L is the average photon detection rate (photons/s). As introduced in Section II-C, the TG mode SPAD receiver effectively alleviates the ISI effect through continuous detection by cyclically enabling the TG window of each sub-array. However, this approach reduces the effective number of SPAD pixels available for photon detection and decreases the received optical power to 25% (only 25% SPAD pixels are available for one sub-SPAD array). In the receiver design of Fig. 5, a 64-SPAD array receiver operated in TG mode is equivalent to a 16-SPAD array receiver without the ISI effect. Consequently, the mean and variance of photon counting probability distribution of the FR mode in the high data rate condition can be expressed by (5a) and (5b), respectively. The mean and variance of photon counting probability distribution of the TG mode can be calculated by (2a) and (2b), respectively, by replacing the total SPAD number with the effective SPAD number and reducing the received optical power and background power by 75%.

The comparisons of the TG mode and the FR mode under different optical power conditions are shown in Fig. 15, and the bit interval is shorter than the dead time. Unlike the CD mode, which achieves higher mean values of photon counting distribution by leveraging its high photon detection ability, the TG mode relies on the less effective detectable SPAD pixels, resulting in a low photon detection ability. Consequently, the photon counting distributions of the TG mode have lower mean values than the FR mode due to the less effective detection pixels. When optical power (P_O) is 1 nW, the mean value of photon counting probability distribution of TG mode is 1, which is lower than that of FR mode (3.5). However, the TG mode offers a solution to the issue of uneven effective detection time caused by the ISI effect in high data rate communication. This can be observed and compared by the variance distributions. As shown in the inserted figure in Fig. 15, the increased gap of the

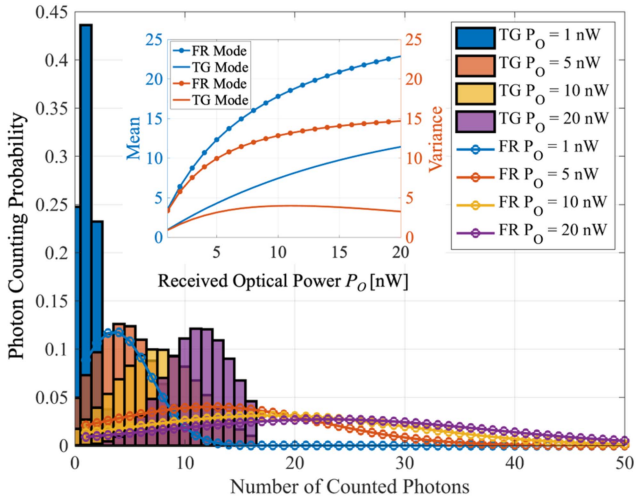

Fig. 15. Photon counting probability distribution of the time-gated (TG) mode and the free-running (FR) mode under variant optical power (64-SPAD array with 10 ns dead time and 5 ns bit interval).

variances comparison with the increased received optical power shows that the condition of uneven detection time caused by ISI effect becomes more serious in the FR mode. Thus, the TG mode exhibits better performance in high optical power conditions. The stronger P_O expands the number range of photon detection of the SPAD. Moreover, due to the ISI effect, the effective detection time of the SPAD also changes greatly. These two factors lead to the trend of the variance of FR mode distribution increasing with the increase of P_O. In contrast, when the ISI effect is eliminated, the variance of TG mode distribution first rises and then falls with the increase of P_O. Specifically, when P_O ranges from 1 nW to 10 nW, the variance value of TG mode increases, because increased P_O expands the range of photon detection number of TG SPAD. However, when P_O is greater than 10 nW, the detected photon number keeps approaching the photon detection limit of TG SPAD, thus decreasing variance value.

Effects from the bit interval are shown in Fig. 16. The advantages of the TG mode are mainly evident in the short bit interval situations. For example, when $T_S = 2.5$ ns, the TG mode distribution has a lower variance value and similar mean value when compared to the FR mode. However, when the bit interval is relatively longer (for example, $T_S = 10$ ns), the FR mode distribution has a higher variance value than the TG mode distribution. Moreover, the mean value of the FR mode distribution (46.56) is much higher than that of the TG mode distribution (17.21) when the bit interval is 10 ns. In such cases, the advantages of the TG mode are no longer apparent, and the FR mode is expected to perform better in the OWC system.

A trade-off needs to be considered in the application of the TG mode. Similar to the CD mode, the TG mode SPAD receiver can efficiently reduce the ISI effect. However, less effective detection pixels due to the cyclic enabling detection mode cause a low photon counting ability. The TG mode is designed for high data rate condition with the feature of the high detection interval consistency. High optical power condition can increase

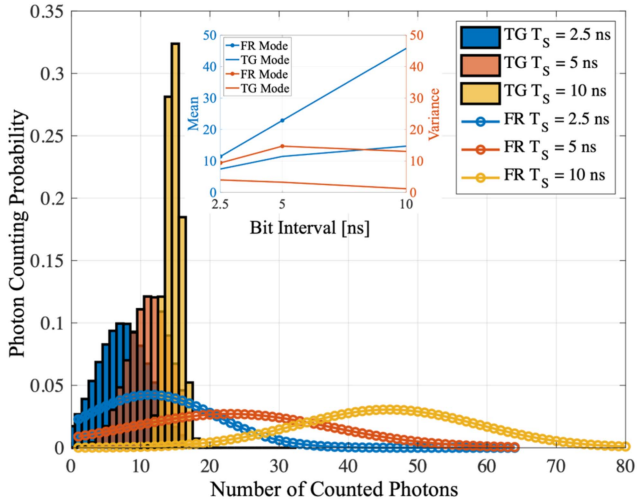

Fig. 16. Photon counting probability distribution of the time-gated (TG) mode and the free-running (FR) mode under variant bit intervals when $P_O = 20$ nW (64-SPAD array with10 ns dead time).

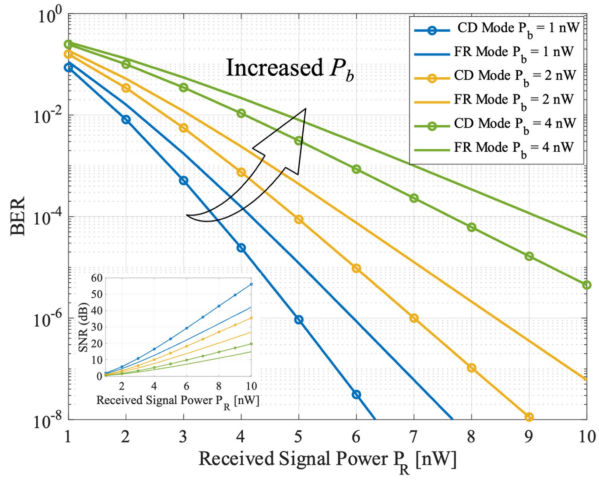

Fig. 17. BER comparisons of the clock-driven (CD) mode and free-running (FR) mode under variant received signal power and background power with $T_S = 15$ ns (64-SPAD array with 10 ns dead time).

the number of detected photons and alleviate the drawback caused by less effective detection pixels in the TG mode. As a result, TG mode receiver has a potential in the OWC application for the conditions of high data rate and high optical power.

IV. BER Performance of SPAD System

A. BER Evaluation

In this research, OOK modulation is used for the simulations of SPAD-based communication system. As the single photon detector, a SPAD receiver judges the signal through the detected photon number. The number of detected photons in a bit interval is compared with a certain threshold. If the detected number of photons is greater than the threshold, the decision device decides that '1' is sent; otherwise, it is decided that '0' is sent. The optimal threshold is a specific threshold value to achieve the lowest BER. It can be expressed as (6) shown at the bottom of this page [17], and the BER of OOK communication with optimum threshold can be expressed as [10]:

$$BER = \frac{1}{2}\sum_{y=y_{th}+1}^{\infty} p_y^0(y) + \frac{1}{2}\sum_{y=0}^{y_{th}} p_y^1(y) \tag{7}$$

where the μ_j, and σ_j^2 are the mean and variance of the photon counting distribution of bit j, $j = 0, 1$, respectively. $p_y^0(y)$and $p_y^1(y)$ denotes the photon counting probabilities of bit 0 and bit 1, respectively. Because of the different photon detected rate (L) for bit '1' and bit '0', their photon condition rates differ. For bit '1', the SPAD receiver receives light from the transmitter and background noise. However, for bit '0', the receiver receives only the background noise. The BER given at (7) can be approximated as [17]:

$$BER \cong Q\left(\sqrt{SNR}\right) \tag{8}$$

$$SNR = \left(\frac{\mu_1 - \mu_0}{\sigma_1 + \sigma_0}\right)^2 \tag{9}$$

$Q(x)$ is the Q-function, which is $Q(x) = 1/\sqrt{2\pi}\int_x^\infty \exp(-\alpha^2/2)\,d\alpha$. Since all noise in this model is integrated into background power (P_b), signal-to-noise ratio (SNR) can be represented by (9). Signal power is defined by the mean of the photon counting distributions of bit '1' and bit '0', noise power comes from the variance of '1' counting distribution and '0' counting distribution. The average photon detection rate of bit '1' and bit '0' can be written as [13]:

$$L_1 = \frac{PDE \times (P_R + P_b)}{Nhf_0} \tag{10a}$$

$$L_0 = \frac{PDE \times P_b}{Nhf_0} \tag{10b}$$

where P_R is the received signal power and P_b is the received background power. N, PDE, h and f_0 are defined in Section III.

B. Simulation Results and Discussions

For this section, we present the numerical results of the BER in different modes, which are simulated and compared. BER comparisons of the CD mode and the FR mode using different variables are illustrated in Figs. 17 and 18. The simulations are performed with T_s set to be 15 ns to ensure the low data rate condition ($T_s > T_d$). As shown in Fig. 17 for three different background powers (P_b), and SNR simulation under same condition is inserted in this figure. As the P_R increases, both the CD mode

$$y_{th} = \frac{\frac{\mu_0}{\sigma_0^2} - \frac{\mu_1}{\sigma_1^2} + \sqrt{\left(\frac{\mu_0}{\sigma_0^2} - \frac{\mu_1}{\sigma_1^2}\right)^2 - \left(\frac{1}{\sigma_0^2} - \frac{1}{\sigma_1^2}\right)\left[\left(\frac{\mu_0^2}{\sigma_0^2} - \frac{\mu_1^2}{\sigma_1^2}\right) + 2\ln\left(\frac{\sigma_0}{\sigma_1}\right)\right]}}{\frac{1}{\sigma_0^2} - \frac{1}{\sigma_1^2}} \tag{6}$$

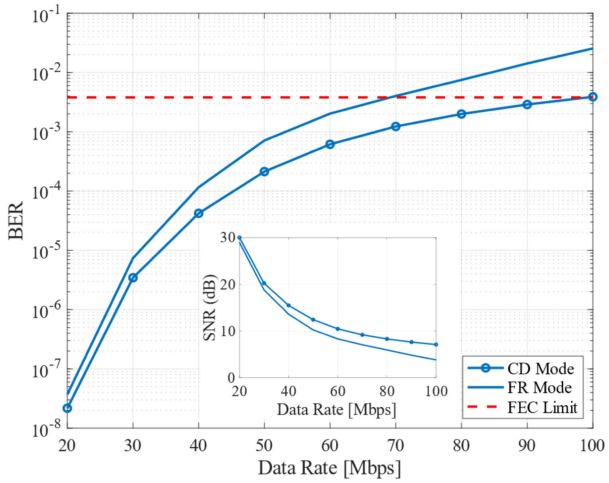

Fig. 18. BER comparisons of the clock-driven (CD) mode and free-running (FR) mode under variant data rate with $P_R = 5$ nW and $P_b = 3$ nW (64-SPAD array with 10 ns dead time).

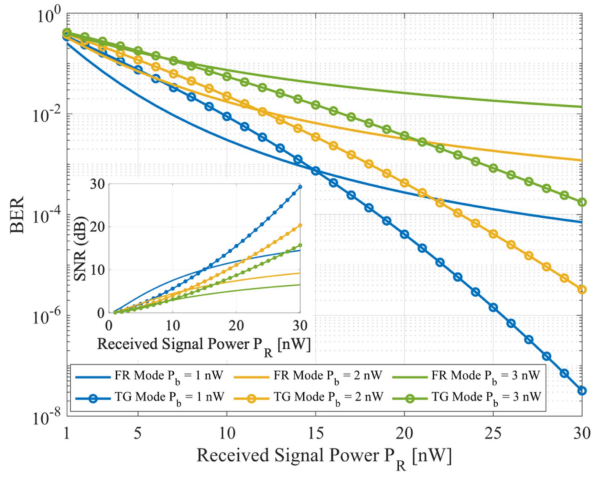

Fig. 19. BER variation comparisons of the time-gated (TG) mode and the free-running (FR) mode under variant received signal power with $T_S = 5$ ns (64-SPAD array with 10 ns dead time).

and FR mode follow a decreasing trend in the BER. However, the increased P_R leads to an increased block time in the FR mode receiver, so its BER reduction is not as high as the CD mode case. That is because the SNR improvement from the increased signal power compensates for the performance decline from the block time, thus increasing the system performance. The CD mode always achieves lower BER than the FR mode under the same P_R condition due to the higher photon counting rate caused by longer effective detection time. This reason can be observed in Fig. 17. That is, compared to the FR mode, the distribution of the CD mode will always have a higher mean value. The ISI effect can be observed through the BER gap between the CD mode and the FR mode. The BER gap is expanded with the incremental P_R value caused by the increasing block time in FR mode and can be observed in Fig. 12(b). In addition, the background power will affect BER's variance to P_R increases. For example, when $P_b = 1$ nW, as the received signal, P_R decreases from 1 ns to 6 ns, the BER decreases by a factor of 10^6 (10^{-1} to10^{-7}), while when $P_b = 4$ nW, the BER drops only by a factor of 10^2. This is because background noise will increase the variance value of distributions in bit 1 and bit 0, leading to the reduced SNR. Another problem caused by background noise is the contribution to block time. Since the CD mode does not have block time, it has a better tolerance to background noise.

Fig. 18 illustrates the BER variance with the increased data rate, and SNR simulation is inserted in this figure. In OOK modulation, the data rate (bps) can be calculated as $\frac{1}{T_s}$. Therefore, the BER increases with the data rate in both the CD mode and the FR mode due to the decreased T_S. As the data rate increases, the symbol interval decreases and the BER increases since the effective detection time decreases. According to (8) and (9), both BER and SNR are strongly affected by the mean values. Under low background power condition, $(\mu_1 - \mu_0)^2 \cong \mu_1$, and as T_S decreases, μ_1 reduces, leading to a performance degradation of the OWC system. The lower performance of the FR mode results from the lower effective detection time due to the ISI effect. The increasing performance gap between the CD mode and the FR mode is because that the ISI effect on the BER performance becomes more and more obvious with the increase of the data rate. This is shown in Fig. 12(a). The higher data rate corresponds to a higher dead time ratio, which will also decrease the effective detection time ratio due to the block time. As a result, at the forward error correction (FEC) limit of 3.8×10^{-3}, the maximum available data rate for the FR mode in this condition is 70 Mbps and the maximum available data rate for the CD mode is 100 Mbps.

When implementing the TG mode for the BER evaluation, we need the high optical power condition and high data rate condition to demonstrate the advantages of the TG mode. In Fig. 19, the T_S is set to be 5 ns, which is shorter than the T_d (10 ns). Since there is no ISI effect, BER variation trend of the TG model is similar to Fig. 17. For the FR mode, the average effective photon detection time per bit interval is very small due to very severe ISI effects, which is even more pronounced at high P_R condition. In this case, the improvement in system performance caused by the increase in signal power will not be significantly greater than the decrease in system performance caused by the ISI effect. Therefore, the improvement in BER of the FR mode saturates as the received signal power increases (see Fig. 19). From the perspective of Monte Carlo simulation and Formulas (8) and (9), since the block time is random, the effective detection time of each bit for FR mode is constantly changing (ranging from 0 to T_S), which will lead to a large variance of photon count distribution of bit 1 and bit 0. In other words, compared to the TG mode, the $(\sigma_1 + \sigma_0)$ value of FR mode is much larger, which will seriously affect the performance of SNR and BER. The TG mode operated in this condition can only achieve better performance than the FR mode in high signal power communication. For example, under the condition of $P_b = 1$ nW, as shown in Fig. 19, the FR mode has lower BER when P_R is lower than 15 nW, while the TG mode perform better when P_R is higher than 15 nW. This is because that the ISI effect is not so obvious when the received optical power is low. Therefore, the FR mode receiver has more effective detection

TABLE I
COMPARISONS OF THREE RECEIVER MODES

	FR mode	CD mode	TG mode
Advantages	1. Simple circuit structure.	1. High photon counting ability. 2. Effective suppression of background noise.	1. High effective detection time 2. low AP impact. 3. Effective suppression of background noise.
Disadvantages	1. High ISI effect in high optical power condition and high data rate condition.	Hight potential AP impact.	Low photon counting ability.
Application Scenarios	High data rate and low optical power condition	Low data rate condition.	High data rate and high optical power condition.

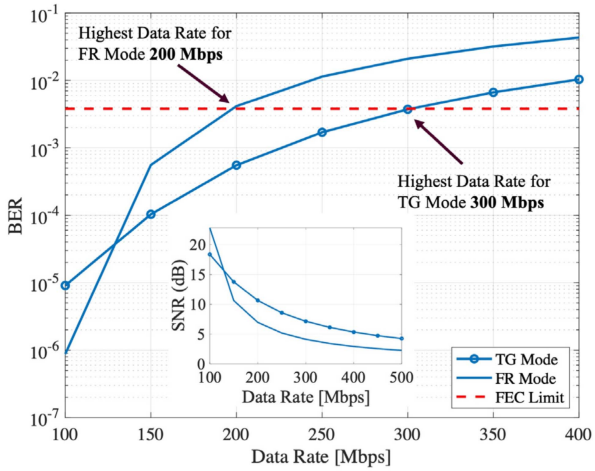

Fig. 20. BER variation comparisons of the time-gated (TG) mode and the free-running (FR) mode under increased date rate with $P_R = 20$ nW and $P_b = 2$ nW (64-SPAD array with 10 ns dead time).

pixels to achieve better photon detection ability. On the contrary, the FR mode suffers from the severer ISI effect in the high optical power condition. The advantage of no ISI effect in TG mode contributes to better performance. The background noise has a negative impact on performance. In the FR mode receiver, the background power causes ISI effect. Under high background power condition, the TG mode shows its advantage. As shown in Fig. 19, TG mode in low background power ($P_b = 1$ nW) requires higher received signal power ($P_R > 15$ nW) to perform better than the FR mode. However, only 5 nW P_R is needed by the TG mode to outperform the FR mode in high background power condition ($P_b = 3$ nW). This is mainly because FR mode is more sensitive to background noise as the background noise will not only increase the variance value of the photon count distributions, but also cause serious ISI effect in FR mode. This shows that the TG mode has a stronger tolerance for the background noise power than FR mode.

The analysis on BER versus data rate is shown in Fig. 20 with an inserted SNR simulation. In a relative low data rate condition such as 100 Mbps, the FR mode has a lower BER. This is due to the weaker ISI effect causes the longer bit interval, leading the FR mode benefits from more effective detection SPAD pixels. The FR mode receiver in this condition has a high mean value in the photon distribution, despite a large variance in the photon count distribution. This is due to the large number of effective SPAD pixels, which enhances the photon detection capability. This conclusion can be obtained from SNR simulation. At a lower data rate, the FR mode receiver has a higher SNR. The ISI effect in the FR mode becomes obvious with the high data rate under a relatively high optical power condition. Therefore, due to the ISI effect, the originally high photon count distribution mean value of FR mode rapidly decreases with the increase of data rate. This leads to a rapid decline in both SNR and BER performance. In TG mode, the variance value of photon count distribution is always low because there is no block time, so the performance of SNR and BER will exceed that of FR mode in high data rate condition. In low data rate conditions, the TG mode exhibits inferior performance compared to the FR mode. This is because the TG mode has fewer effective pixels than the FR mode, and the ISI in FR mode is not significant at low data rate conditions. Consequently, in low data rate conditions, TG mode fails to demonstrate its advantages. As shown in Fig. 20, the FR mode has a higher BER than the TG mode when the data rate is higher than 135 Mbps.

C. Discussion

In this section, a comparison of the performance of SPAD receivers based on the OWC model is presented, with a summary of the outcomes provided in Table I. The FR mode has a simpler circuit structure as no signal generation circuit is required. However, a notable disadvantage of FR mode is the high ISI effect that occurs in high optical power and high data rate conditions, as indicated by the results of the communication model used in this paper. The CD mode receiver demonstrates high photon counting ability and effective suppression of background noise. However, the variable dead time in the CD mode introduces uncertainty in afterpulsing impact, resulting in a higher noise level in high data rate communication and potentially affecting system performance. The TG mode offers high effective detection time and low afterpulsing probability even under high data rate conditions. However, the TG receiver may suffer from low photon counting ability in low optical power conditions due to fewer effective SPAD pixels. Hence, high data rate and high optical power are necessary conditions to fully exploit the advantages of the TG mode.

V. Conclusion

In this paper, one SPAD front-end circuit optimized for OWC application is designed and measured, featuring with very low dead time (2.6 ns) and adjustable hold-off time. Based on this SPAD circuit two new modes, the clock-driven (CD) mode and time-gated (TG) mode, are proposed to improve the performance of the OWC system. Additionally, a novel block time simulation method is first introduced in this research to reveal the factors causing ISI effect and applied into an OWC model. The CD mode and the TG mode are evaluated by this OWC model, demonstrating their advantages and limitations.

The CD-mode SPAD receiver is characterized by periodic resetting of SPAD pixels, effectively avoiding dead time extension to adjacent bit intervals and mitigating the ISI effect. This results in a higher photon count ability compared to the free-running (FR) mode, which is indicated by larger mean values in the photon counting probability distributions. BER simulations show that the CD-mode receiver outperforms the FR-mode receiver in low data rate communication and exhibits higher tolerance to background noise. The TG-mode SPAD receiver divides the SPAD array into 4 sub-SPAD-arrays and realizes the cyclic enablement detection, which effectively reduces the ISI effect as the dead time in one sub-array does not affect other sub-arrays. Comparisons between the TG mode and FR mode reveal that the TG mode exhibits lower variance values in the photon counting probability distributions, indicating higher consistency in effective detection time, and performs better under high optical power and high data rate conditions. However, the less effective detection pixels in TG mode causes a low photon detection ability, thus leading to a low performance under the condition of low data rate and low optical power.

It is worth noting that the three operation modes (FR mode, CD mode, TG mode) presented in this paper are suitable for different communication scenarios. The future research could focus on combining these modes to further expand the application scenarios of SPAD receivers and enhance the performance of OWC systems.

References

[1] S. Zhu, X. Chen, X. Liu, G. Zhang, and P. Tian, "Recent progress in and perspectives of underwater wireless optical communication," *Prog. Quantum Electron.*, vol. 73, 2020, Art. no. 100274, doi: 10.1016/j.pquantelec.2020.100274.

[2] H. Chen et al., "Toward long-distance underwater wireless optical communication based on a high-sensitivity single photon avalanche diode," *IEEE Photon. J.*, vol. 12, no. 3, Jun. 2020, Art. no. 7902510, doi: 10.1109/JPHOT.2020.2985205.

[3] J. Kosman et al., "29.7 A 500Mb/s -46.1dBm CMOS SPAD receiver for laser diode visible-light communications," in *Proc. IEEE Int. Solid- State Circuits Conf.*, 2019, pp. 468–470, doi: 10.1109/ISSCC.2019.8662427.

[4] W. Matthews, Z. Ahmed, W. Ali, and S. Collins, "A 3.45 Gigabits/s SiPM-based OOK VLC receiver," *IEEE Photon. Technol. Lett.*, vol. 33, no. 10, pp. 487–490, May 2021, doi: 10.1109/LPT.2021.3069802.

[5] S. Huang, C. Chen, R. Bian, H. Haas, and M. Safari, "5 Gbps optical wireless communication using commercial SPAD array receivers," *Opt. Lett.*, vol. 47, pp. 2294–2297, 2022, doi: 10.1364/OL.454994.

[6] M. J. Deen and P. K. Basu, *Silicon Photonics: Fundamentals and Devices*. Hoboken, NJ, USA: Wiley, 2012.

[7] W. Jiang and M. J. Deen, "Random telegraph signal in n^+/p-well CMOS single-photon avalanche diodes," *IEEE Trans. Electron Devices*, vol. 68, no. 6, pp. 2764–2769, Jun. 2021, doi: 10.1109/TED.2021.3070557.

[8] W. Jiang, R. Scott, and M. J. Deen, "High-speed active quench and reset circuit for SPAD in a standard 65 nm CMOS technology," *IEEE Photon. Technol. Lett.*, vol. 33, no. 24, pp. 1431–1434, Dec. 2021, doi: 10.1109/LPT.2021.3124989.

[9] W. Jiang, R. Scott, and M. J. Deen, "Improved noise performance of CMOS poly gate single-photon avalanche diodes," *IEEE Photon. J.*, vol. 14, no. 1, Feb. 2022, Art. no. 6802208, doi: 10.1109/JPHOT.2021.3128055.

[10] E. Sarbazi, M. Safari, and H. Haas, "The impact of long dead time on the photocount distribution of SPAD receivers," in *Proc. IEEE Glob. Commun. Conf.*, 2018, pp. 1–6, doi: 10.1109/GLOCOM.2018.8647814.

[11] I. M. Antolovic, S. Burri, C. Bruschini, R. Hoebe, and E. Charbon, "Nonuniformity analysis of a 65-kpixel CMOS SPAD imager," *IEEE Trans. Electron Devices*, vol. 63, no. 1, pp. 57–64, Jan. 2016, doi: 10.1109/TED.2015.2458295.

[12] I. M. Antolovic, C. Bruschini, and E. Charbon, "Dynamic range extension for photon counting arrays," *Opt. Exp.*, vol. 26, no. 17, pp. 22234–22248, Aug. 2018, doi: 10.1364/OE.26.022234.

[13] S. Huang and M. Safari, "Time-gated photon counting receivers for optical wireless communication," *J. Lightw. Technol.*, vol. 39, no. 22, pp. 7113–7123, Nov. 2021, doi: 10.1109/JLT.2021.3112828.

[14] W. Jiang, Y. Chalich, R. Scott, and M. J. Deen, "Time-gated and multi-junction SPADs in standard 65 nm CMOS technology," *IEEE Sensors J.*, vol. 21, no. 10, pp. 12092–12103, May 2021, doi: 10.1109/JSEN.2021.3063319.

[15] J. Liu, W. Jiang, and M. J. Deen, "Time-gated circuit for SPAD-based OWC," in *Proc. IEEE Photon. Conf.*, 2022, pp. 1–2, doi: 10.1109/IPC53466.2022.9975721.

[16] Y. Mu, X. Du, C. Wang, Z. Ye, and Y. Zhu, "Gate-width optimisation based on time-gated single photon avalanche diode receiver for optical wireless communications," *Electronics*, vol. 11, no. 14, Jul. 2022, Art. no. 2218, doi: 10.3390/ELECTRONICS11142218.

[17] E. Sarbazi, M. Safari, and H. Haas, "The bit error performance and information transfer rate of SPAD array optical receivers," *IEEE Trans. Commun.*, vol. 68, no. 9, pp. 5689–5705, Sep. 2020, doi: 10.1109/TCOMM.2020.2993374.

[18] R. Enne, B. Steindl, M. Hofbauer, and H. Zimmermann, "Fast cascoded quenching circuit for decreasing afterpulsing effects in 0.35-μm CMOS," *IEEE Solid State Circuits Lett.*, vol. 1, no. 3, pp. 62–65, Mar. 2018, doi: 10.1109/LSSC.2018.2827881.

[19] D. P. Palubiak, Z. Li, and M. J. Deen, "Afterpulsing characteristics of free-running and time-gated single-photon avalanche diodes in 130-nm CMOS," *IEEE Trans. Electron Devices*, vol. 62, no. 11, pp. 3727–3733, Nov. 2015, doi: 10.1109/TED.2015.2475126.

[20] S. Lindner, S. Pellegrini, Y. Henrion, B. Rae, M. Wolf, and E. Charbon, "A high-PDE, backside-illuminated SPAD in 65/40-nm 3D IC CMOS pixel with cascoded passive quenching and active recharge," *IEEE Electron Device Lett.*, vol. 38, no. 11, pp. 1547–1550, Nov. 2017, doi: 10.1109/LED.2017.2755989.

[21] D. Bronzi, S. Tisa, F. Villa, S. Bellisai, A. Tosi, and F. Zappa, "Fast sensing and quenching of CMOS SPADs for minimal afterpulsing effects," *IEEE Photon. Technol. Lett.*, vol. 25, no. 8, pp. 776–779, Apr. 2013, doi: 10.1109/LPT.2013.2251621.

[22] X. Jiang et al., "Afterpulsing effects in free-running InGaAsP single-photon avalanche diodes," *IEEE J. Quantum Electron.*, vol. 44, no. 1, pp. 3–11, Jan. 2008, doi: 10.1109/JQE.2007.906996.

[23] M. Kokkonen and S. Pietilä, "A new bit synchronization method for a GPS receiver," in *Proc. IEEE Position Location Navigation Symp.*, 2002, pp. 85–90, doi: 10.1109/PLANS.2002.998893.

[24] S. Huang, S. M. Patanwala, J. Kosman, R. K. Henderson, and M. Safari, "Optimal photon counting receiver for sub-dead-time signal transmission," *J. Lightw. Technol.*, vol. 38, no. 18, pp. 5225–5235, Sep. 2020, doi: 10.1109/JLT.2020.3000723.

[25] E. Sarbazi, M. Safari, and H. Haas, "Statistical modeling of single-photon avalanche diode receivers for optical wireless communications," *IEEE Trans. Commun.*, vol. 66, no. 9, pp. 4043–4058, Sep. 2018, doi: 10.1109/TCOMM.2018.2822815.

[26] E. Sarbazi, M. Safari, and H. Haas, "On the information transfer rate of SPAD arrays," in *Proc. IEEE Wireless Commun. Netw. Conf.*, 2020, pp. 1–6, doi: 10.1109/WCNC45663.2020.9120696.

[27] C.-C. Chen, "Effect of detector dead time on the performance of optical direct-detection communication links," *Telecommun. Data Acquisition Prog. Rep.*, vol. 42–93, pp. 146–154, Jan./Mar. 1988.